PLOS PATHOGENS

RESEARCH ARTICLE

SARS-CoV-2 ORF8 modulates lung inflammation and clinical disease progression

Marisa E. McGrath[1¤], Yong Xue[2], Louis Taylor[1], Carly Dillen[1], Jeremy Ardanuy[1], Norberto Gonzalez-Juarbe[2], Lauren Baracco[1], Raymond Kim[2], Rebecca Hart[2], Nacyra Assad-Garcia[2], Sanjay Vashee[2], Matthew B. Frieman[1] *

1 Center for Pathogen Research, Department of Microbiology and Immunology, University of Maryland School of Medicine, Baltimore, Maryland, United States of America, 2 J. Craig Venter Institute, Rockville, Maryland, United States of America

¤ Current address: Vaccine Research Center, NIAID, NIH, Bethesda, Maryland, United States of America
* mfrieman@som.umaryland.edu

Abstract

The virus severe acute respiratory syndrome coronavirus 2, SARS-CoV-2, is the causative agent of the current COVID-19 pandemic. It possesses a large 30 kilobase (kb) genome that encodes structural, non-structural, and accessory proteins. Although not necessary to cause disease, these accessory proteins are known to influence viral replication and pathogenesis. Through the synthesis of novel infectious clones of SARS-CoV-2 that lack one or more of the accessory proteins of the virus, we have found that one of these accessory proteins, ORF8, is critical for the modulation of the host inflammatory response. Mice infected with a SARS-CoV-2 virus lacking ORF8 exhibit increased weight loss and exacerbated macrophage infiltration into the lungs. Additionally, infection of mice with recombinant SARS-CoV-2 viruses encoding ORF8 mutations found in variants of concern reveal that naturally occurring mutations in this protein influence disease severity. Our studies with a virus lacking this ORF8 protein and viruses possessing naturally occurring point mutations in this protein demonstrate that this protein impacts pathogenesis.

Author summary

The SARS-CoV-2 genome is composed of various genes that are responsible for replication of its genome, making virions as well as aiding the virus in replicating in host cells. The virus expresses several viral proteins during infection that are also thought to modulate the host response to the virus. Identifying the role of these proteins in infection and how they affect both viral replication and host response to infection is important to understand how SARS-CoV-2 causes disease. One of these proteins, ORF8, is mutated across many variant lineages and its function is unclear. Both the role of ORF8 in pathogenesis and how these mutations could be advantageous to viral fitness are unknown. We have found that mutations in ORF8 across variants recapitulate the loss of function phenotype of an ORF8 deletion virus and affect inflammation during infection. Mutations found in variants that cause a loss of function of ORF8 increase inflammation in our animal model suggesting that these mutations may play the same role in humans. Differences in ORF8

sequences of variants may significantly impact disease severity in humans and alter transmission kinetics so that mechanistic studies of its function are important to understand as SARS-CoV-2 continues to be spread.

Introduction

A cluster of viral pneumonia cases was first observed in Wuhan, Hubei province, China in December of 2019. The causative agent of this pneumonia was later revealed to be a novel coronavirus, now known as severe acute respiratory syndrome coronavirus 2, or SARS-CoV-2. The virus quickly spread, leading to the declaration of a pandemic in 2020.[1] The pandemic, known as the COVID-19 pandemic, has now claimed over 7 million lives as of March 2024.[2] Despite the widespread deployment of vaccines, the pandemic persists, with the emergence of viral variants greatly affecting vaccine effectiveness.

SARS-CoV-2 is a beta coronavirus that shares significant homology to SARS-CoV, which was responsible for viral pneumonia cases originating in China in 2002.[3,4] The enveloped virus possesses a 30kb positive-sense RNA genome. The genome is functionally divided into thirds, with the 5′ end of the genome encoding the replication machinery and the 3′ end encoding the structural proteins Spike (S), Membrane (M), Envelope (E), and Nucleocapsid (N). Interspersed with the structural proteins are a variety of accessory proteins.[5] All coronaviruses possess accessory proteins, although the number of accessory proteins and their functions vary amongst the members of the coronavirus family. The accessory proteins of coronaviruses do follow a functional theme, with many of the proteins being implicated in antagonism of both Type I Interferon (IFN) signaling and activity of Interferon-Stimulated Genes (ISGs), and others being implicated in interference with the cellular autophagy process which it uses to acquire membrane sources for viral replication.[6]

Many of the accessory proteins of SARS-CoV-2 possess high sequence homology, of around 80%, to accessory proteins found in SARS-CoV.[7] The ORF8 protein of SARS-CoV-2 is the most divergent accessory protein from SARS-CoV, with the proteins only possessing 40% amino acid identity.[4] A main difference between the two is that the ORF8 of SARS-CoV possesses a 29 base pair deletion that divides the ORF8 into two separate ORFs, known as ORF8a and ORF8b.[4,6] The function of SARS-CoV ORF8a and ORF8b is hypothesized to involve the degradation of IRF3.[8] SARS-CoV-2 ORF8 has numerous hypothesized functions, including down-regulation of MHC class I on the cell surface, modulation of spike incorporation into virions, and agonism of IL-17 receptor signaling.[9–11] Deletions in ORF8 in clinical isolates of SARS-CoV-2 have also been identified in Singapore and Taiwan, demonstrating the high level of selective pressure on this accessory protein.[12]

Our previous work with accessory protein deletion viruses of SARS-CoV-2 revealed that an ORF8 deletion virus resulted in increased lung inflammation when compared to a clinical isolate.[13] To further characterize the impact of ORF8 in clinical disease progression, we infected mice with two different doses of our WA-1ΔORF8 virus and compared weight loss and lung inflammation to a clinical isolate of WA-1. Our results show that the absence of ORF8 impacts inflammation at both doses, causing increased immune cell infiltration. As every variant that has emerged since B.1.1.7 in late 2020 possesses either one or more ORF8 mutations, we aimed to characterize the impact of these naturally occurring ORF8 mutations on viral pathogenesis by synthesizing recombinant WA-1 virus containing variant ORF8 genes of B.1.1.7, B.1.351, and P.1 to characterize the functional consequences of these mutations in a murine model.

Materials and methods

Ethics statement

All virus experiments and recombinant virus creation was approved by the Institutional Biosafety Committee at The University of Maryland, Baltimore. All animals were cared for according to the standards set forth by the Institutional Animal Care and Use Committee at the University of Maryland, Baltimore in protocol # AUP-00000349.

Infectious clone construction and rescue

SARS-CoV-2 DNA Fragment Cloning. The cloning of SARS-CoV-2 DNA fragments and transformation-associated recombination (TAR) assembly of genomes were performed as previously described.[13] Briefly, the SARS-CoV-2 WA1 genome was cloned into seven individual DNA fragments: 1a-1, 1a-2, 1a-3, 1b-1, 1b-2, S, and AP. The TAR vectors were PCR amplified from pCC1BAC-his3 and used to clone each fragment. Yeast transformants were patched on synthetic dropout medium plates, and correct junctions between the fragment and vector were confirmed by detection PCR and Sanger sequencing.[14] Plasmid DNAs of the fragments were isolated from E. coli and used for complete genome assembly or further modifications.

ORF8 Deletion in AP Fragment. The generation of ORF8 deletions in the AP fragment was achieved using in vitro CRISPR-Cas9 digestion and TAR assembly, as described in our previous publication.[13] The process involved Cas9 target site identification, sgRNA transcription, AP fragment digestion, and TAR assembly with an oligo in yeast via spheroplast transformation.

Generation of AP Fragments with ORF8 Single Mutations and ORF8 Genes in B.1.1.7 and P.1 Variants. To generate ORF8 single mutations (S84L, E92K) and ORF8 genes in B.1.1.7 and P.1 variants, short fragments were amplified using Platinum SuperFi II DNA polymerase (Thermo Fisher) and the wild-type AP fragment as a template. The ORF8 single mutations and ORF8 genes in B.1.1.7 and P.1 variants were introduced by primers into each amplicon, which had 30–35 bp of homology at each end between the adjacent fragments. The amplicons were then digested with DpnI (NEB) to remove template DNA and purified with a Qiagen PCR purification kit.

Subsequently, 50 fmol of each amplicon and 15 fmol of the YCpBAC vector were assembled using the standard Gibson assembly reaction (NEB), transformed into *E. coli* DH10B competent cells (Thermo Fisher), and plated on LB medium containing 12.5 mg/ml chloramphenicol. The presence of desired mutations or ORF8 genes in B.1.1.7 and P.1 variants was confirmed through colony PCR and Sanger sequencing (GeneWiz). Plasmid DNAs containing the desired modifications were isolated from *E. coli* using the Purelink HiPure Plasmid Midiprep Kit (Thermo Fisher).

Complete genome assembly. The complete genome assembly was performed as previously described.[12] Briefly, the TAR vector for the complete genome was generated by assembling a pCC1-ura3 amplicon, a CMV promoter amplicon, a BamHI fragment, a polyA fragment, and an HDVR+BGH region into circular DNA in yeast by TAR. SARS-CoV-2 DNA fragment plasmids were digested with I-SceI (NEB) to release the overlapping fragments from the backbones, and the complete genome vector was linearized by BamHI (NEB) digestion. The fragments and complete genome vector were mixed with yeast spheroplasts for TAR assembly. Transformants were patched on SD-URA plates, and positive clones were screened by PCR. The subsequent DNA isolation from yeast, transformation into, and extraction from *E. coli* followed the same procedure as for DNA fragment clones.

For a detailed description of the complete genome assembly, please refer to our previous publication[13].

Virus Reconstitution. 24 hours prior to transfection, 5e4 VeroTMPRSS2 cells (*ATCC*, Manassas, VA) were plated per well in 1mL of VeroTMPRSS2 media (DMEM (*Quality Biological*, Gaithersburg, MD), 10% FBS (*Gibco*, Waltham, MA), 1% Penicillin-Streptomycin (*Gemini Bio Products*, Sacramento, CA), 1% L-Glutamine (*Gibco*, Waltham, MA)). For transfection, 5µg of the infectious clone and 100ng of a SARS-CoV-2 WA-1 nucleoprotein expression plasmid were diluted in 100µL of OptiMEM (*Gibco*, Waltham, MA). 3µL of TransIT-2020 (*Mirus Bio*, Madison, WI) was added and the reactions were incubated for 30 minutes prior to addition to the cells in the BSL-3. Cells were checked for cytopathic effect (CPE) 72–96 hours after transfection and the supernatant collected for plaque purification. For plaque purification, 6e5 VeroTMPRSS2 cells were plated in a 6-well plate in 2mL of VeroTMPRSS2 media 24 hours prior to infection. 25µL of this supernatant was then serial diluted 1:10 in DMEM and 200µL of this supernatant was added to the VeroTMPRSS2 cells. The cells were rocked every 15 minutes for 1 hour at 37˚C prior to overlay with 2mL of a solid agarose overlay (EMEM (*Quality Biological*, Gaithersburg, MD), 10% FBS, 1% Penicillin-Streptomycin, 1% L-Glutamine, 0.4% w/v SeaKem agarose (*Lonza Biosciences*, Morrisville, NC). Cells were incubated for 72 hours at 37˚C and 5% CO_2 and individual plaques were picked and then transferred to a well of a 6-well plate with 4e5 VeroTMPRSS2 cells in 3mL VeroTMPRSS2 media. After 48 hours, successful plaque picks were assessed by presence of CPE. 1mL of a well showing CPE was transferred to a T175 with 8e6 VeroTMPRSS2 cells in 30mL of VeroTMPRSS2 media and the virus stock was collected 48 and 72 hours after. The stocks were then titered by plaque assay.

Titering of virus stocks, growth curve samples, tissue homogenates by plaque assay

The day prior to infection, 2e5 VeroTMPRSS2 cells were seeded per well in a 12-well plate in 1mL of VeroTMPRSS2 media. Tissue samples were thawed and homogenized with 1mm beads in an Omni Bead ruptor (*Omni International Inc.*, Kennesaw, GA) and then spun down at 21,000xg for 2 minutes. A 6-point dilution curve was prepared by serial diluting 25µL of sample 1:10 in 225µL DMEM. 200µL of each dilution was then added to the cells and the plates were rocked every 15 minutes for 1 hour at 37˚C. After 1hr, 2mL of a semi-solid agarose overlay was added to each well (DMEM, 4%FBS, 0.06% UltraPure agarose (*Invitrogen*, Carlsbad, CA). After 72 hours at 37˚C and 5% CO_2, plates were fixed in 2% PFA for 20 minutes, stained with 0.5mL of 0.05% Crystal Violet and 20% EtOH, and washed 2x with H_2O prior to counting of plaques. The titer was then calculated. For tissue homogenates, this titer was multiplied by 40 based on the average tissue sample weight being 25mg.

Growth curve infection and sample processing

The day prior to infection, 1.5e5 VeroTMPRSS2 cells or 1.5e5 A549-ACE2 cells (Courtesy of Dr. Brad Rosenberg, *Icahn School of Medicine at Mount Sinai)* were seeded in a 12-well plate in 1.5mL of VeroTMPRSS2 media or A549-ACE2 media (DMEM, 10% FBS, 1% penicillin-streptomycin). The day of infection, cells were washed with 500µL of DMEM and the volume of virus needed for an M.O.I. of 0.01 was diluted in 100µL DMEM and added to a well in triplicate. The plates were rocked every 15 minutes for 1hr at 37˚C. After 1hr, the inoculum was removed, the cells were washed with 500µL of complete media and then 1.5mL of complete media was added to each well. 300µL of this supernatant was taken as the 0hr timepoint and replaced with fresh media. 300µL of supernatant was pulled and replaced with fresh media at 0hr, 6hr, 24hr, 48hr, 72hr, and 96hr timepoints. This supernatant was then titered.

Infection of hACE2-k18 mice

All animals were cared for according to the standards set forth by the Institutional Animal Care and Use Committee at the University of Maryland, Baltimore in protocol # AUP-00000349. On Day 0, 12–14 week old hACE2 transgenic K18 mice (K18-hACE2) (*Jackson Labs*, Bar Harbor, ME) were anesthetized interperitoneally with 50μL ketamine (1.3mg/mouse)/xylazine (0.38mg/mouse). The K18-hACE2 mice were then inoculated with either 1e2 or 1e3 PFU of each virus in 50μL PBS. The mock infected mice received 50μL PBS only. Mice were then weighed every day until the end of the experiment. Mice were euthanized with iso-flurane on day 2, 4 and 7. From each mouse, the left lung was collected in PFA for histology and the right lung was split in half with one half placed in PBS for titer and one half placed in TRIzol for RNA extraction.

RT-qPCR of tissue homogenates

Samples were homogenized in an Omni Bead ruptor in TRIzol and then the RNA was extracted from 300μL of each sample using the Direct-zol RNA miniprep kit (*Zymo Research*, Irvine, CA). 2μL of isolated RNA from each sample was then converted to cDNA using the RevertAID first strand cDNA synthesis kit (*Thermo Fisher*, Waltham, MA) in a 20μL total reaction volume. For qPCR for SARS2 Rdrp, 20μL reactions were prepared using 2μL cDNA, 1μL of 10mM Rdrp Forward primer (10006860, *Integrated DNA Technologies*, Coralville, IA), 1μL of Rdrp Reverse primer (10006881, *Integrated DNA Technologies*, Coralville, IA), and 10μL of 2x SYBR Green (*Thermo Fisher*, Waltham, MA). The reactions were then run on a 7500 Fast Dx Real-Time PCR Instrument (4357362R, *Applied Biosystems*, Waltham, MA). For qPCR for murine GAPDH, 20μL reactions were prepared using 2μL cDNA, 1μL of a 20x murine GAPDH primer (MM.pt.39a.1, *Integrated DNA Technologies*, Coralville, IA), and 10μL of 2x SYBR Green. The reactions were then run on a QuantStudio 5 Real-Time PCR Instrument (A28133, *Applied Biosystems*, Waltham, MA).

Histology & Immunohistochemistry

Mouse lungs were fixed in 4% paraformaldehyde (PFA) in PBS for at least 48 hours. These lungs were then sent to the University of Maryland Baltimore Histology core facility for paraffin embedding, sectioning into 5 micro-meter sections and staining with hematoxylin and eosin (H&E) staining.

Lungs were scored in a blinded fashion with a 0 to 5 score given, 0 being no inflammation and 5 being the highest degree of inflammation. Interstitial inflammation and peribronchiolar inflammation were scored separately. Scores were then averaged for the overall inflammation score.

Cytokine arrays

The concentration of lung RNA was quantified using a Nanodrop (NanoVue Plus, *GE Healthcare*, Chicago, IL). 400ng of RNA was converted to cDNA using the Qiagen RT^2 First Strand Kit (330404, *Qiagen*, Hilden, Germany). The cDNA was analyzed with the Qiagen RT^2 Mouse Cytokines and Chemokines array (PAMM-150Z, *Qiagen*, Hilden, Germany). Reactions were run on a QuantStudio 5 Real-Time PCR Instrument (A28133, *Applied Biosystems*, Waltham, MA). The results were analyzed with the Qiagen analysis spreadsheet provided with the kit.

RNA sequencing and analysis

Library preparation and sequencing was performed by the University of Maryland Institute of Genome Sciences (Baltimore, MD, USA). After RNA extraction, as described above,

transcriptomic libraries were generated and sequenced on an Illumina NovaSeq 6000 (S4 flow cell, 100bp paired-end; *Illumina*, San Diego, CA). Raw data is available in the NCBI SRA under the accession number PRJNA857920. Reads were preprocessed using cutadapt v3.4, then aligned to the murine genome (assembly GRCm38) using STAR v2.7.8a.[15,16] Genes with at least a mean count of 10 reads in at least one condition were subject to differential expression analysis with DESeq2 v4.1.0 followed by pathway analysis using Ingenuity Pathway Analysis (*Qiagen*, Hilden, Germany).[17] Genes were only considered for follow-up if the magnitude of differential expression was at least 2-fold in either direction and the difference in expression between conditions was significant ($p<0.05$) after multiple testing correction.

Immunostaining for immune cell markers

Histological samples were processed according to optimized protocols established by *HistoWiz* (Brooklyn, NY, USA). Samples were stained using antibodies for SARS-CoV-2 nucleocapsid, the macrophage marker F4-80 (*Cat #14-4801-82, Clone BM8*), and the neutrophil marker Ly6G (*Cat #ab25377, Clone RB6-8C5*). Images were taken using the *HistoWiz* software. IHC was quantified in ImageJ for percent of sections that had specific antibody staining. Five fields per mouse were quantified and graphed.

Flow cytometry

Single cells were isolated from lungs using the Lung Dissociation Kit, mouse and gentleMACS Dissociator (Miltenyi Biotec). Lungs were placed in C tubes (Miltenyi Biotec) containing 2.2 mL Buffer S, 15 µL of Enzyme A, and 100 µL of Enzyme D. Lungs were run on m_lung_01 and allowed to digest for 30 minutes at 37˚C followed by running m_lung_02. Cell suspensions were filtered on a 70-µm filter (BD), and cells were pelleted by centrifugation. Red blood cells were lysed in ammonium-chloride-potassium lysis buffer (Quality Biological, Inc.) and subsequently washed with PBS containing 3% FBS. Approximately, $1x10^6$ cells were plated and washed twice with PBS containing. Cells were stained for viability using the Live/Dead Fixable NIR Dead Cell Stain Kit (Molecular Probes). Cells were washed with PBS containing 3% FBS. Cells were stained with antibody cocktails made in BD Horizon Brilliant Stain Buffer (BD). The antibodies used were as follows: CD45 Alexa Fluor 700 (BioLegend, clone 30-F11), CD11b Brilliant Violet 650 (BioLegend, clone M1/70), Ly6G Brilliant Violet 785 (BioLegend, clone 1A8), Ly6C Brilliant Violet 510 (BioLegend, clone HK1.4), CD3 BUV 563 (BD, clone 145-2C11), CD4 FITC (BioLegend, clone GK1.5), CD8a APC (BioLegend clone 53–6.7), CD19 PE (BioLegend clone 6D5), and NK1.1 Pacific Blue (BioLegend, clone PK136), CD65 Brilliant Violet 605 (BioLegend, clone X54-5/7.1), CD103 BUV 661 (BD, clone 2e7), Siglec-H BUV 563 (BD, clone 440c), and Siglec-F Brilliant Violet 711 (BD, clone E50-2440). Stained cells were washed twice and fixed for 1 hour in FluoroFix (BioLegend). Fixed cells were washed once in PBS containing 3% FBS and resuspended in PBS containing 3% FBS. Samples were acquired (approximately 50,000 events) using the Aurora-UV spectral flow cytometer (Cytek), and data were analyzed using FCS Express analysis software (DeNova Software, Pasadena, CA).

Statistical analysis

All statistical analyses were carried out using the GraphPad Prism software (GraphPad Software, San Diego, CA, USA) or R version 4.1.1.[18] The cutoff value used to determine significance was $p\leq0.05$ for all tests. The statistical tests run were unpaired t-tests assuming unequal variances, or one-way ANOVA followed by T-test with Bonferroni correction, where indicated. For the differential expression analysis, reported p-values are the result of the Wald test after Benjamini-Hochberg correction, as calculated by DESeq2 v4.1.0.[17]

Biosafety approval

All virus experiments and recombinant virus creation was approved by the Institutional Biosafety Committee at The University of Maryland, Baltimore.

Results

Infection of K18-hACE2 mice with WA-1ΔORF8 results in increased weight loss and increased lung inflammation compared to mice infected with WA-1

SARS-CoV-2 ORF8 has been proposed to have several functions. To directly assess the role of ORF8 in pathogenesis we produced a recombinant SARS-CoV-2 virus lacking the complete sequence of ORF8 and compared pathogenesis of this mutant to the wildtype SARS-CoV-2 strain WA-1. Our previous work with an ORF8 deletion virus revealed a difference in lung inflammation when compared to mice infected with the wildtype virus. To further investigate this phenotype, we infected 12–14 week old K18-hACE2 transgenic mice with either 1e2 PFU or 1e3 PFU of either WA-1 or WA-1ΔORF8. We assessed weight loss daily, lung viral loads by plaque assay, and viral RNA levels by qPCR for RdRp were measured at days 2, 4, and 7 post-infection. At both doses, mice infected with WA-1ΔORF8 lost weight a day earlier than mice infected with the full-length WA-1 (**Fig 1A and 1B**). There was no mortality observed at either dose by day 7 post infection. By day 7, mice infected with the ORF8 deletion virus had 5–7% more weight loss compared to mice infected with the full-length virus (**Fig 1A and 1B**). Despite the increased weight loss, no differences in lung viral titer were observed at the 1e2 PFU dose (**Fig 1C**). In the 1e3 PFU dose, we find that WA-1ΔORF8 infected mice have a statistically significant one log decrease in lung viral titer at Day 4 compared to the WA-1 infected mice (p = 0.012, **Fig 1C**). Levels of viral RNA by qPCR for RdRp in the WA-1ΔORF8 mice were measured and no statistically significant changes were observed at both doses across all days (**Fig 1D**). At the doses and timepoints analyzed in previous studies, there was insignificant or non-detectable virus titer in the brains of mice, so brain titer was not analyzed or quantified here [13].

The lungs from these mice were fixed and stained for histological analysis. Despite the fact that mice infected with 1e2 WA-1ΔORF8 lost more weight than mice infected with 1e2 WA-1, the lungs exhibited similar levels of inflammation (**Fig 2A and 2B**). At the dose of 1e3 PFU, mice infected with the deletion virus exhibited increased inflammation in the lungs at days 2, 4, and 7 post-infection. This inflammation included infiltration of cells into the alveolar space and both thickening and sloughing of cells of the major airways (**Fig 2A**). Histological scoring of the lungs revealed statistically significant differences, with the lungs of the mice infected with 1e3 WA-1ΔORF8 exhibiting increased inflammation at days 2, 4, and 7 post-infection (Day 2 p = 0.027, Day 4 p = 0.0013, Day 7 p = 0.0027).

Transcriptomic analysis of the lungs of K18-hACE2 mice infected with WA-1ΔORF8 or WA-1 reveals an upregulation of macrophage signaling pathways and a concurrent increase in the population of macrophages in the lungs by immunohistochemistry

To investigate the pathways associated with the increased inflammation seen in the lungs of mice infected with the WA-1ΔORF8 virus, we performed an analysis of the inflammatory cytokines and chemokines in the lungs of these mice at Days 2, 4 and 7, finding that many cytokines and chemokines associated with innate immune cell chemotaxis and cytokine storm signaling were upregulated early in infection (**Table 1**). Notably, we observed more significant
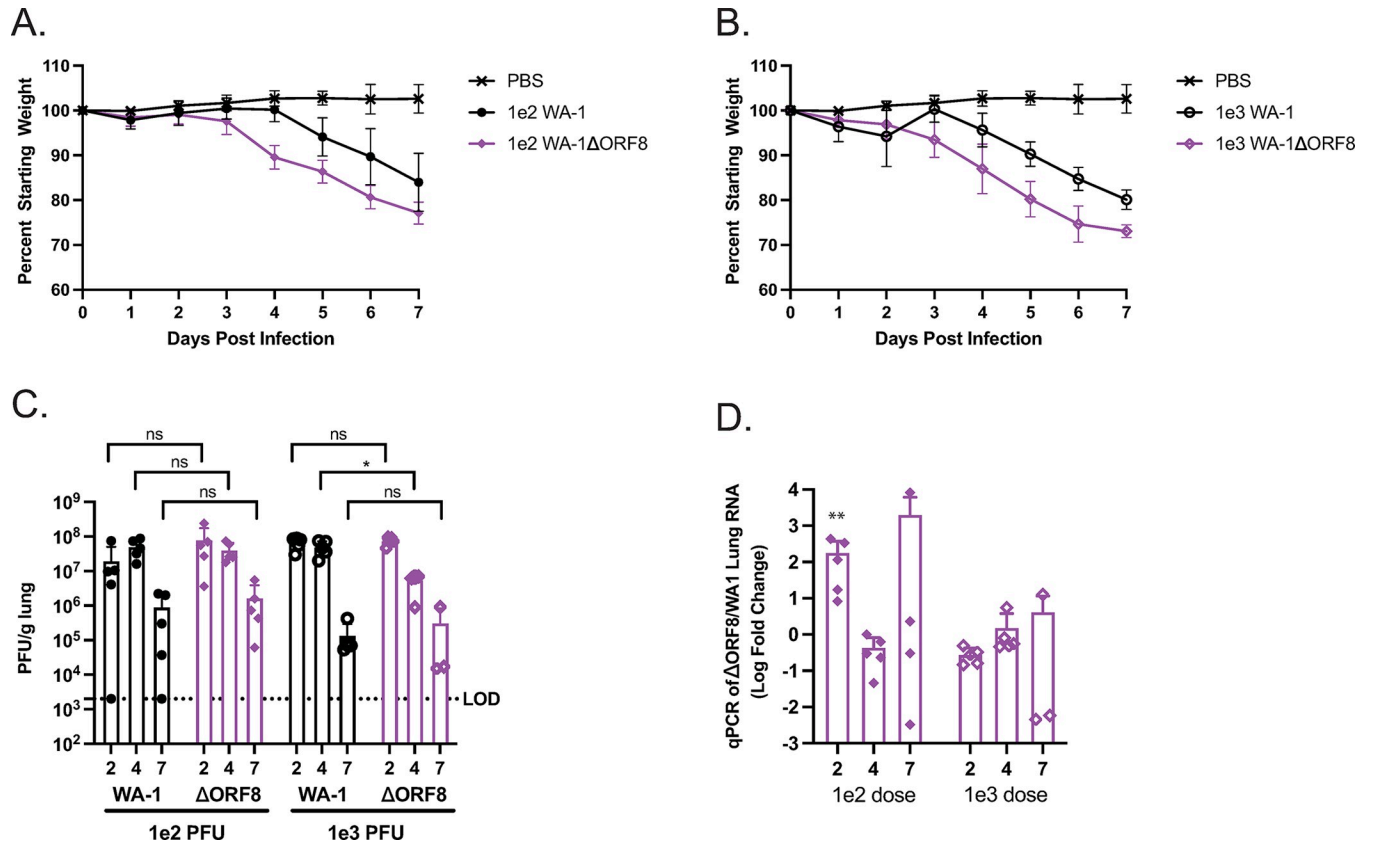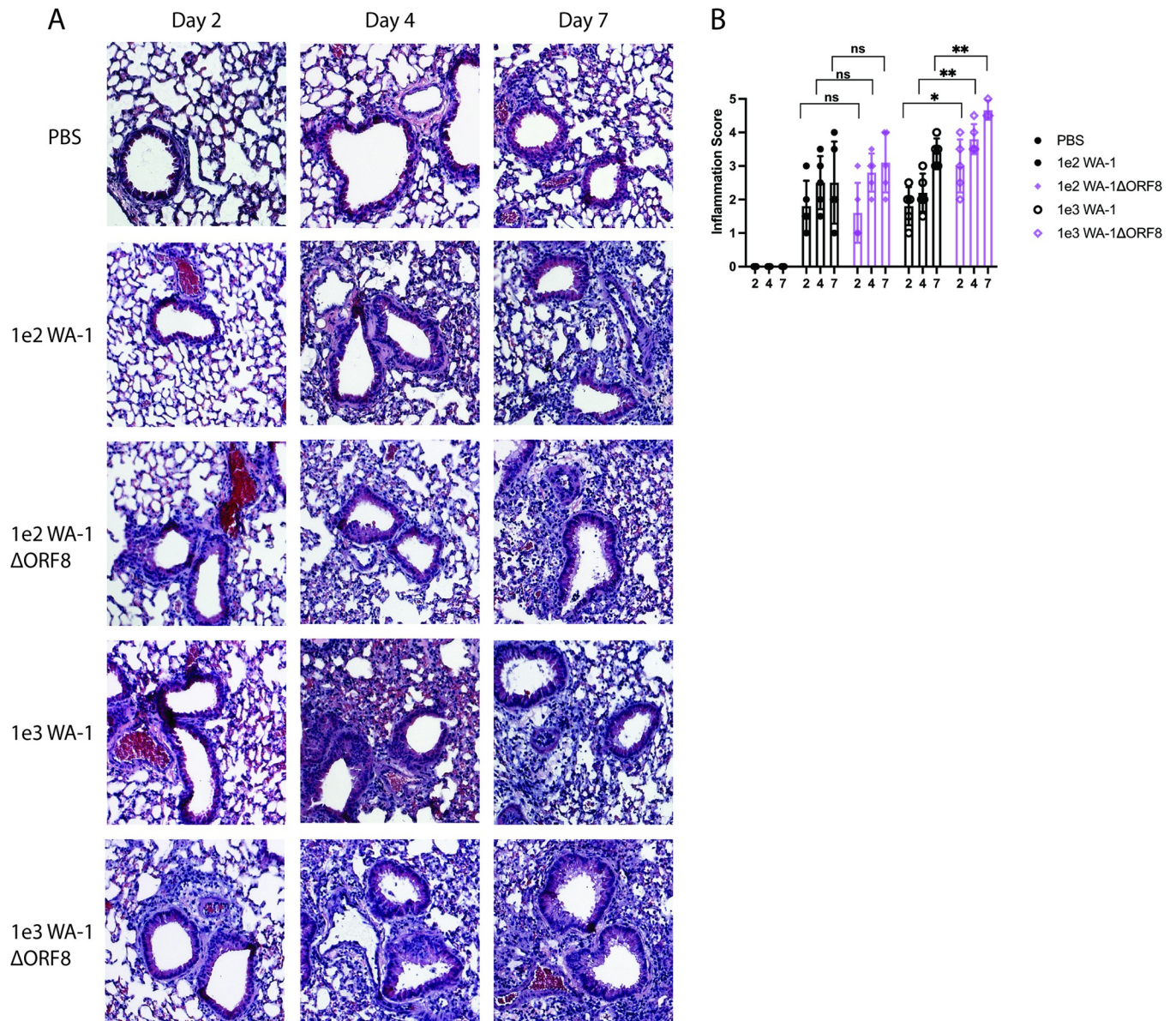
Fig 1. Pathogenesis of K18/hACE2 mice infected with WA1 or WA-1ΔORF8 K18/hACE2 mice infected with either WA1 or WA-1ΔORF8 to determine differences in pathogenesis. A. Weight loss of mice infected with either PBS, 1e2 PFU of SARS-CoV-2 WA-1, or 1e2 PFU of SARS-CoV-2 WA-1ΔORF8 (n = 15 mice per virus). B. Weight loss of mice infected with either PBS, 1e3 PFU of SARS-CoV-2 WA-1, or 1e3 PFU of SARS-CoV-2 WA-1ΔORF8. (n = 15 mice per virus) C. Live virus titers by PFU/g lung in mice infected with either WA-1 or WA-1ΔORF8. (n = 5 mice per timepoint) D. Viral RNA levels of RdRp expressed as a fold change relative to the comparable dose of WA-1 (n = 5 mice per timepoint). Sample comparisons with significant differences are shown. (*, $p \leq 0.05$; **, $p \leq 0.005$; ***, $p \leq 0.0005$, ns = not significant).

changes in the lower dose (1e2 PFU) as compared to the higher dose (1e3 PFU), which we hypothesize is due to the increased amount of virus masking any subtler changes.

Specifically, we noticed an induction of key inflammatory proteins that recruit or stimulate macrophages and monocytes in the lungs like CCL1, CCL2, CCL4, CCL7 and CXCL10 (**Table 1**). This demonstrates an increase in chemokines involved with recruiting macrophages and neutrophils, which correlates with what is observed in the H&E scoring in **Fig 2**. For a further analysis of the affected pathways, we isolated the RNA from the lungs of mice infected with either the deletion virus or the full-length virus and performed RNA-seq. Transcriptomic analysis of mouse lungs infected with WA-1 or WA-1ΔORF8 at days 2, 4 and 7 post infection identified key changes to the immune response in the lungs dependent on the virus (**Fig 3A– 3C**). In particular, neutrophil associated responses were similar across time points for both viruses. Classical macrophage (M1 macrophages) associated genes were differentially regulated early in infection at day 2. WA-1 infected lungs have a muted induction of M1 macrophage associated genes while WA-1ΔORF8 infected mice have significant and rapid induction of M1 macrophage associated genes. This includes CD68, CD80 and CD86 (**Fig 3D**). M2 macrophage associated genes were also differentially upregulated in WA-1ΔORF8 infected mice with ARG1, CLEC7a and RETNLB significantly upregulated compared to WA-1 infected mice (**Fig 3E**). Comparison of fold change of WA-1ΔORF8 / WA-1 infected mice for these selected

Fig 2. Lung histology and histological scores of K18/hACE2 mice infected with WA-1 or WA- 1ΔORF8. Lungs from infected mice at day 2, 4 and 7 post infection were fixed and sectioned for staining with H&E. A. H&E staining of the lungs of mice infected with WA-1 or WA-1ΔORF8. Representative images of each group, n = 5 mice per virus and timepoint. B. Histological scoring of the lungs of mice infected with either WA-1ΔORF8 or WA-1. Scoring described in methods section (n = 5 mice per timepoint) Sample comparisons with significant differences are shown. (*, $p \leq 0.05$; **, $p \leq 0.005$; ***, $p \leq 0.0005$).

https://doi.org/10.1371/journal.ppat.1011669.g002

genes demonstrates early induction of the macrophage/monocyte induced genes in the WA-1ΔORF8 infected mice (**Fig 3F and 3G**). This suggests that the inflammation observed in lungs is a result of macrophage activation and recruitment that may be impairing lung function to cause more severe disease, as we observe with the WA-1ΔORF8 virus.

Since we observed an increase in neutrophil and macrophage signaling pathways, we wanted to determine the localization of these cells in the lungs, particularly at the dose of 1e3 PFU at day 7 post-infection where we saw the most significant differences in lung inflammation between the mice infected with the deletion virus and the mice infected with the full-length virus. We performed immunohistochemistry on the lungs of these mice, staining for

Table 1. Fold changes of inflammatory cytokines and chemokines of mouse lungs on Day 2, Day 4, and Day 7. The values in bold are statistically significant.

Experimental Group	10^2 PFU WA-1ΔORF8			10^3 PFU WA-1ΔORF8		
Control Group	10^2 PFU WA-1			10^3 PFU WA-1		
	Fold Change Relative to Control Group					
Gene	Day 2	Day 4	Day 7	Day 2	Day 4	Day 7
Adipoq	1.29	**0.43**	1.27	0.63	1.30	1.63
Bmp2	1.33	**0.15**	0.69	0.79	**2.05**	0.60
Bmp4	0.51	0.61	0.65	2.00	1.31	0.95
Bmp6	**0.44**	0.54	0.59	1.86	0.72	0.89
Bmp7	0.83	**0.23**	0.81	0.74	1.65	1.89
Ccl1	**3.06**	**0.18**	1.75	**0.27**	1.70	0.73
Ccl11	1.73	**0.46**	1.38	0.51	1.02	0.96
Ccl12	**5.86**	0.94	0.84	**0.48**	**0.32**	**0.34**
Ccl17	0.58	0.77	0.91	0.95	**4.98**	**3.65**
Ccl19	1.41	0.66	0.94	1.43	1.12	0.98
Ccl2	**29.46**	0.80	1.14	1.25	**0.41**	0.81
Ccl20	**3.99**	**0.41**	1.45	0.85	1.94	0.63
Ccl22	**3.81**	**0.10**	1.95	1.28	0.92	1.54
Ccl24	**3.06**	**0.11**	0.61	**0.30**	**3.32**	**2.67**
Ccl3	**5.14**	**0.24**	0.71	1.72	0.75	0.67
Ccl4	**5.13**	**0.34**	0.62	1.78	0.58	0.81
Ccl5	**2.01**	**0.31**	0.59	1.32	0.64	0.76
Ccl7	**11.40**	1.67	0.92	**3.45**	0.65	0.82
Cd40lg	**2.32**	**0.09**	0.52	**0.48**	1.13	1.85
Cd70	**3.06**	**0.16**	1.63	**0.30**	**2.33**	0.98
Cntf	**2.24**	**0.48**	0.90	0.84	1.31	1.44
Csf1	1.97	0.66	0.84	**2.22**	1.13	1.28
Csf2	1.46	**0.24**	0.95	**0.40**	**2.11**	1.03
Csf3	**3.56**	**0.32**	1.54	0.53	**2.77**	1.15
Ctf1	1.17	**0.19**	**0.47**	0.56	1.87	0.90
Cx3cl1	0.60	**0.16**	0.89	1.43	0.97	0.59
Cxcl1	**2.37**	0.51	1.28	1.49	1.25	1.72
Cxcl10	**12.61**	**0.45**	0.81	**2.74**	0.52	0.71
Cxcl11	**3.94**	**0.05**	1.37	**0.42**	0.88	**2.32**
Cxcl12	**0.47**	0.89	1.32	**2.35**	1.98	1.04
Cxcl13	**6.68**	**2.26**	**2.50**	1.03	1.60	1.20
Cxcl16	**3.49**	0.79	1.00	0.63	0.61	0.73
Cxcl3	**5.38**	**0.33**	1.39	0.59	1.64	1.97
Cxcl5	**13.04**	**0.24**	**4.00**	**0.44**	0.78	1.06
Cxcl9	**6.41**	**0.25**	1.55	**0.50**	**0.29**	1.04
Fasl	**5.81**	**0.21**	0.84	**0.50**	1.11	1.05
Gpi1	**0.45**	1.10	0.88	1.25	1.05	1.39
Hc	1.25	**0.28**	**0.38**	**0.43**	**0.47**	0.58
Ifna2	**3.06**	**0.06**	0.61	**0.36**	0.88	1.91
Ifng	**3.87**	**0.07**	1.01	0.55	0.63	0.57
Il10	**3.34**	**0.18**	0.91	1.04	0.83	1.31
Il11	**2.35**	0.54	0.84	0.69	**3.95**	1.53
Il12a	1.25	**0.36**	0.95	**2.36**	1.43	1.15
Il12b	**2.19**	**0.27**	1.17	0.51	0.62	1.57

(Continued)

Table 1. (Continued)

Experimental Group	10^2 PFU WA-1ΔORF8			10^3 PFU WA-1ΔORF8		
Control Group	10^2 PFU WA-1			10^3 PFU WA-1		
	Fold Change Relative to Control Group					
Gene	Day 2	Day 4	Day 7	Day 2	Day 4	Day 7
Il13	**2.72**	**0.16**	1.77	**0.33**	1.97	1.28
Il15	**2.40**	**0.26**	0.87	1.65	0.58	1.04
Il16	1.36	**0.22**	0.92	**0.47**	0.82	0.58
Il17a	**3.40**	**0.11**	0.65	**0.33**	**3.06**	**2.67**
Il17f	**5.00**	**0.09**	0.61	**0.44**	1.21	1.64
Il18	1.53	**0.31**	0.94	0.66	0.81	0.84
Il1a	**6.97**	**0.27**	1.09	**0.41**	0.53	0.88
Il1b	**6.14**	**0.21**	1.44	**0.50**	0.62	1.20
Il1rn	**5.10**	**0.16**	0.79	1.11	**0.39**	0.65
Il2	**3.06**	**0.08**	0.64	**0.29**	**3.32**	**3.76**
Il21	**3.06**	**0.10**	1.20	**0.37**	**3.32**	1.54
Il22	**2.55**	**0.09**	0.61	**0.22**	**2.97**	**2.67**
Il23a	**3.37**	**0.15**	1.29	**0.45**	**4.14**	1.51
Il24	**3.07**	**0.14**	**0.49**	**0.32**	1.13	0.87
Il27	**5.18**	**0.11**	1.18	0.56	1.77	**2.19**
Il3	**3.06**	**0.09**	0.61	**0.31**	**3.32**	**2.67**
Il4	1.73	**0.12**	1.11	0.63	1.90	**3.62**
Il5	**2.57**	**0.15**	0.92	**0.40**	1.79	1.40
Il6	**9.17**	**0.15**	1.39	0.75	**0.37**	**5.94**
Il7	**4.58**	**0.16**	1.10	**0.38**	1.18	1.11
Il9	**3.06**	**0.09**	0.61	**0.31**	**3.32**	**2.67**
Lif	**4.32**	**0.37**	1.32	0.64	1.28	**2.23**
Lta	**2.80**	**0.24**	1.22	**0.38**	1.81	**2.71**
Ltb	1.45	**0.36**	0.82	0.58	0.58	0.79
Mif	0.83	1.39	1.09	1.24	1.52	1.46
Mstn	**2.81**	**0.11**	0.61	**0.24**	**3.17**	**2.79**
Nodal	**3.06**	**0.11**	0.61	**0.28**	**3.32**	**5.47**
Osm	1.37	**0.13**	1.58	**0.37**	1.04	**2.49**
Pf4	1.18	1.13	0.81	0.57	**4.12**	**2.63**
Ppbp	0.57	1.36	0.54	1.56	1.51	1.25
Spp1	1.02	**3.96**	1.55	**0.36**	**2.02**	1.46
Tgfb2	0.90	**0.34**	0.81	1.08	0.75	1.19
Thpo	**2.87**	**0.06**	1.01	**0.28**	1.13	0.98
Tnf	1.42	**0.23**	0.91	0.69	0.70	1.58
Tnfrsf11b	1.24	**0.08**	0.90	0.70	1.85	1.08
Tnfsf10	1.64	0.60	0.81	1.71	0.58	0.59
Tnfsf11	**3.98**	**0.15**	1.16	**0.24**	**3.81**	**2.59**
Tnfsf13b	0.60	**0.48**	0.66	1.72	1.00	1.02
Vegfa	**0.45**	**0.44**	0.62	1.53	0.78	1.01
Xcl1	**26.00**	**0.20**	1.42	**0.45**	**0.33**	0.79
Actb	0.81	**2.67**	0.86	1.65	1.20	1.21
B2m		**3.70**	1.18	**0.44**	0.63	0.74
Gapdh	1.55	**0.22**	1.23	0.52	1.02	0.85
Gusb	0.61	0.66	0.91	1.32	1.18	1.29
Hsp90ab1	**0.43**	0.70	0.88	**2.02**	1.09	1.02

https://doi.org/10.1371/journal.ppat.1011669.t001
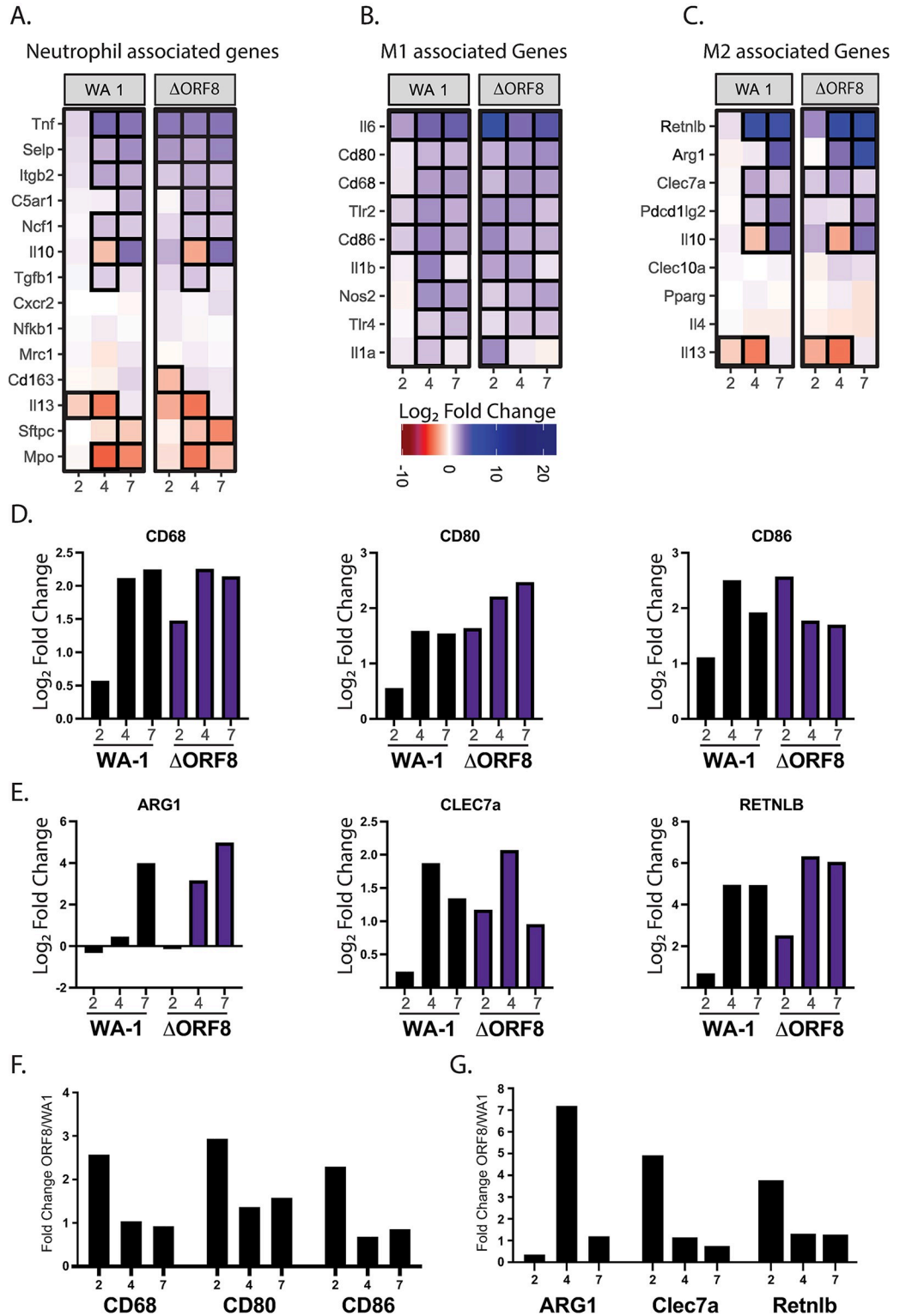
Fig 3. Differentially expressed genes in WA-1 and WA-1ΔORF8 infection. A, B and C. Selected genes associated with neutrophils (A), M1 macrophages (B) and M2 macrophages C) are shown as heat maps. Differentially expressed pathways at Day 2, 4 and 7 are shown for infections at a dose of 10^3 PFU per mouse. All Log$_2$ fold change is relative to a PBS control infection mouse at the same timepoint. A scale of fold change is shown below. D. Graphing of Log$_2$ fold change for select genes in each set in B and C that show dynamic changes in heat map. F and G. Fold change of transcriptomic data of ΔORF8 compared to WA1 infections at each time point for selected genes.

the markers Ly6G to identify neutrophils and F4-80 to identify macrophages. At day 7 post-infection, mice infected with WA-1 and WA-1ΔORF8 had similar insignificant levels of Ly6G positive neutrophils in the lungs. However, the lungs of the mice infected with the WA-1ΔORF8 virus had significantly more macrophages in the lungs at this timepoint, which correlates with the upregulation of macrophage signaling pathways seen in the lungs of these mice early in infection by RNASeq analysis (**Fig 4A**). Immunohistochemical staining of sections for nucleocapsid demonstrated equivalent levels of antigen positive cells across mice, however staining of macrophages (anti-F4/80) demonstrated an increase in macrophage numbers in WA-1ΔORF8 compared to WA-1 infected lungs. Quantification of positive cells demonstrates a significant difference in F4/80 positive cells in the WA-1ΔORF8 lungs compared to WA-1 lungs (Fig 4B). There was no statistical difference in localization of the virus by nucleocapsid staining at this timepoint, with the majority of the virus being cleared from the large airways and localizing to the alveolar space.

We quantified the percentage change of macrophages in lungs by flow cytometry to corroborate the immunohistochemistry quantitation. After infection of WA-1 and WA-1ΔORF8 in mice for 7 days, lungs were dissociated and macrophage populations were identified by gating first on live single cell populations and then identifying a CD45+, CD11b+, CD64+ and Ly6G-population of cells (**Figs 4C and S1**). Macrophages were increased from 3.1% to 5% in WA-1 and WA-1ΔORF8, respectively. This correlates with the 2-fold increase in F4/80 positive macrophages found by immunohistochemical staining compared to WA-1.

## Naturally occurring mutations in ORF8 result in increased levels of inflammation in the lungs

With the emergence of the variants of SARS-CoV-2, we noticed an increase in the incidence of naturally occurring mutations in the ORF8 protein. To determine if these naturally occurring mutations affect inflammation, we generated recombinant WA-1 viruses containing variant ORF8 genes. We produced four viruses to study including a WA-1 virus with the B.1.1.7 ORF8, a WA-1 virus with the P.1 ORF8, a virus with the point mutation S84L and a virus with the point mutation E92K. The B.1.1.7 ORF8 protein contains four mutations, with the most notable being the introduction of a premature stop codon at amino acid 27 out of 121. The point mutation S84L occurs in all variants of SARS-CoV-2, beginning with the emergence of B.1.1.7 in December of 2020. The P.1 ORF8 contains the S84L mutation and an additional E92K mutation, which we also synthesized individually.

After producing this panel of WA-1 viruses containing mutant ORF8 genes, we determined the growth of the viruses in VeroTMPRSS2 cells. All of the viruses grew comparably (**Fig 5A**). We next infected K18-hACE2 mice, first with the WA-1 virus containing the B.1.1.7 ORF8 and a virus containing the single mutation of ORF8 S84L. We compared their weight loss and lung titers to mice infected with either WA-1 or the WA-1ΔORF8 virus. Mice infected with the WA-1ΔORF8 virus and the B.1.1.7 ORF8 virus, lost weight a day earlier and by day 7 lost 5–7% more weight than the mice infected with WA-1. The mice infected with the WA-1 ORF8 S84L virus began losing weight the same day as the WA-1 mice, but by day 7 lost 5–7% more weight than the mice infected with WA-1, similar to the WA-1ΔORF8 mice (**Fig 5B**). As we saw in mice infected with the deletion virus, there were no significant differences in lung titer by plaque assay amongst most of the groups at all time points (**Fig 5C**). The only group that showed a difference in lung titer is the WA-1 ORF8 S84L infected mice which had a reduction in virus by day 7 post infection. We then infected K18-hACE2 mice with the WA1 virus containing the P.1 ORF8 and a WA-1 virus containing only the ORF8 E92K mutation. The mice infected with the P.1 ORF8 containing virus exhibited an intermediate weight loss phenotype
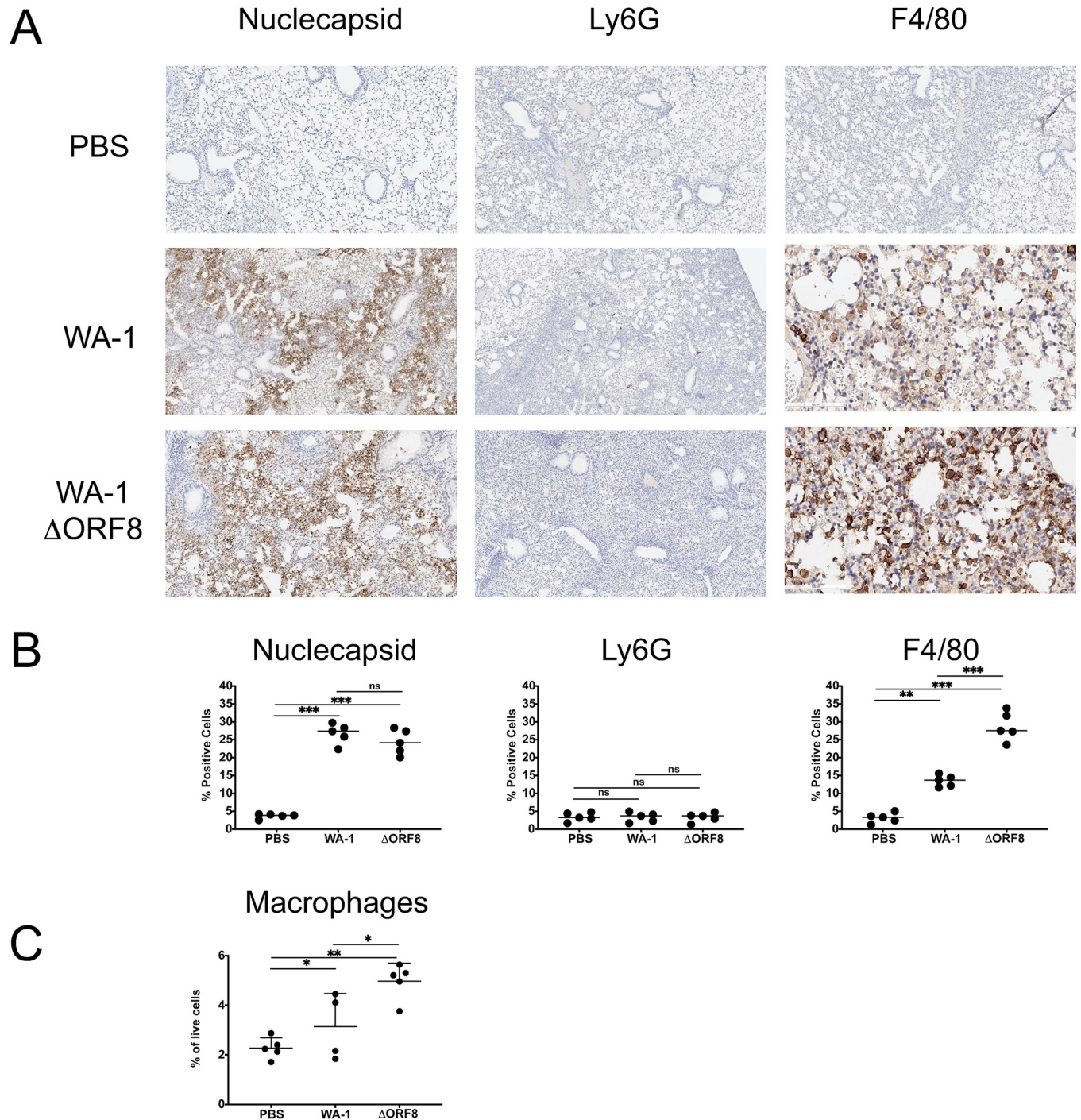
Fig 4. Staining for neutrophils (Ly6G), macrophages (F4-80) and nucleocapsid in the lungs of WA-1 and WA-1ΔORF8 infected mice. A. Lungs from mice infected with 10^3 PFU of WA-1 and WA-1ΔORF8 infected mice at 7-day post infection were fixed and stained for neutrophils (anti-Ly6G), macrophages (anti-F4/80) or SARS-CoV-2 nucleocapsid (anti-N). Brown stain denotes positive antibody labeling of respective protein targets. Representative images shown of 5 mice at day 7 post infection. B. Quantitation of IHC for neutrophils (anti-Ly6G), macrophages (anti-F4/80) or SARS-CoV-2 nucleocapsid (anti-N). Quantitation in Image J. C. Flow cytometry of % of macrophages of live cells in the lungs after 7 days of infection with either WA-1 or WA-1ΔORF8. (*, p≤ 0.05; **, p≤0.005; ***, p≤0.0005).

https://doi.org/10.1371/journal.ppat.1011669.g004
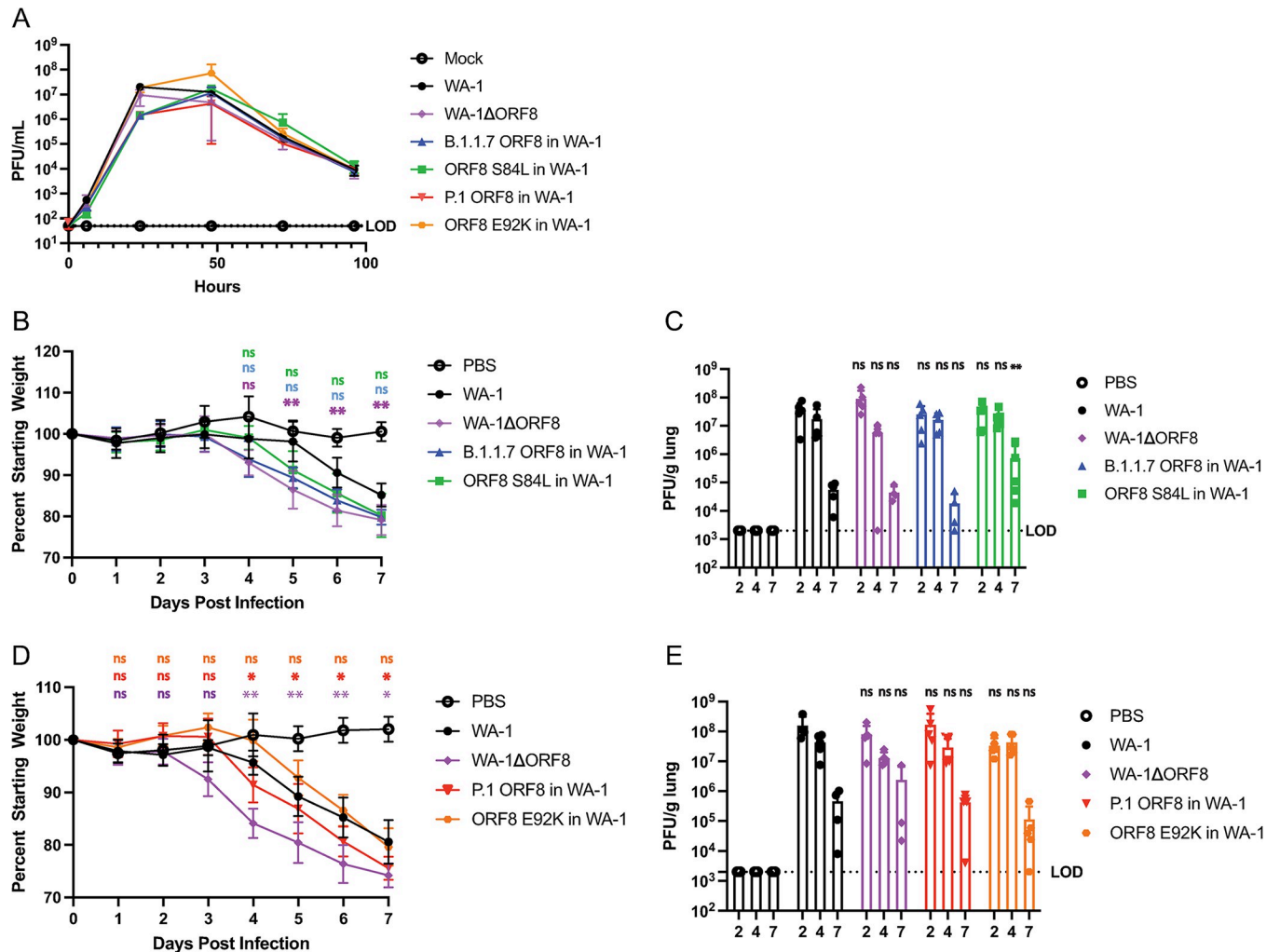
Fig 5. Infection of K18-hACE2 mice with variant ORF8 in WA-1 viruses. Cells and K18/hACE2 mice were infected with either 10^3 PFU of WA1, WA-1ΔORF8, B.1.1.7 ORF8 in WA-1, or ORF8 S84L in WA-1 to determine differences in replication and pathogenesis. A. SARS-CoV-2 viruses expressing variant ORF8 genes were evaluated for growth by infection of VeroTMPRSS2 cells at MOI of 0.01 across a timecourse of infection. Supernatants were titered by plaque assay on VeroTMPRSS2 cells. B. Weight loss of K18-hACE2 mice infected with 10^3 PFU of WA-1, WA-1ΔORF8, B.1.1.7 ORF8 in WA-1, or ORF8 S84L in WA-1. (n = 5 mice/timepoint) C. Lung titers by plaque assay of K18-hACE2 mice infected with WA-1, WA-1ΔORF8, B.1.1.7 ORF8 in WA-1, or ORF8 S84L in WA-1. D. Weight loss of K18-hACE2 mice infected with WA-1, WA-1ΔORF8, P.1 ORF8 in WA-1, or ORF8 E92K in WA-1. E. Lung titers by plaque assay of K18-hACE2 mice infected with WA-1, WA-1ΔORF8, P.1 ORF8 in WA-1, or ORF8 E92K in WA-1. In 5B and 5D, colors of significance markers correspond to the weight curve of each virus. Colors of the lines represent the statistical significance of that mutant compared to WT WA-1. In 5C and E, the statistical significance is relative to the WA1 control to assess statistical significance. (*, p≤ 0.05; **, p≤0.005; ***, p≤0.0005).

compared to the WA-1 and the WA-1ΔORF8 mice, while the mice infected with the ORF8 E92K containing virus exhibited a weight loss phenotype that more closely resembled that seen in WA-1 infected mice (**Fig 5D**). As with the previous set of ORF8 mutant WA-1 viruses, we did not see significant differences in lung titers by plaque assay amongst all of the infected mice (**Fig 5E**).

We next examined the histopathological data of the lungs of mice infected with the panel of viruses. We noted significant inflammation in the lungs of all infected mice. However, as expected, the mice infected with the virus containing the B.1.1.7 ORF8, which contains a severely truncated ORF8, results in inflammation that is higher than the wildtype virus infected mice. These lungs contain a significant number of cells in the alveolar space and
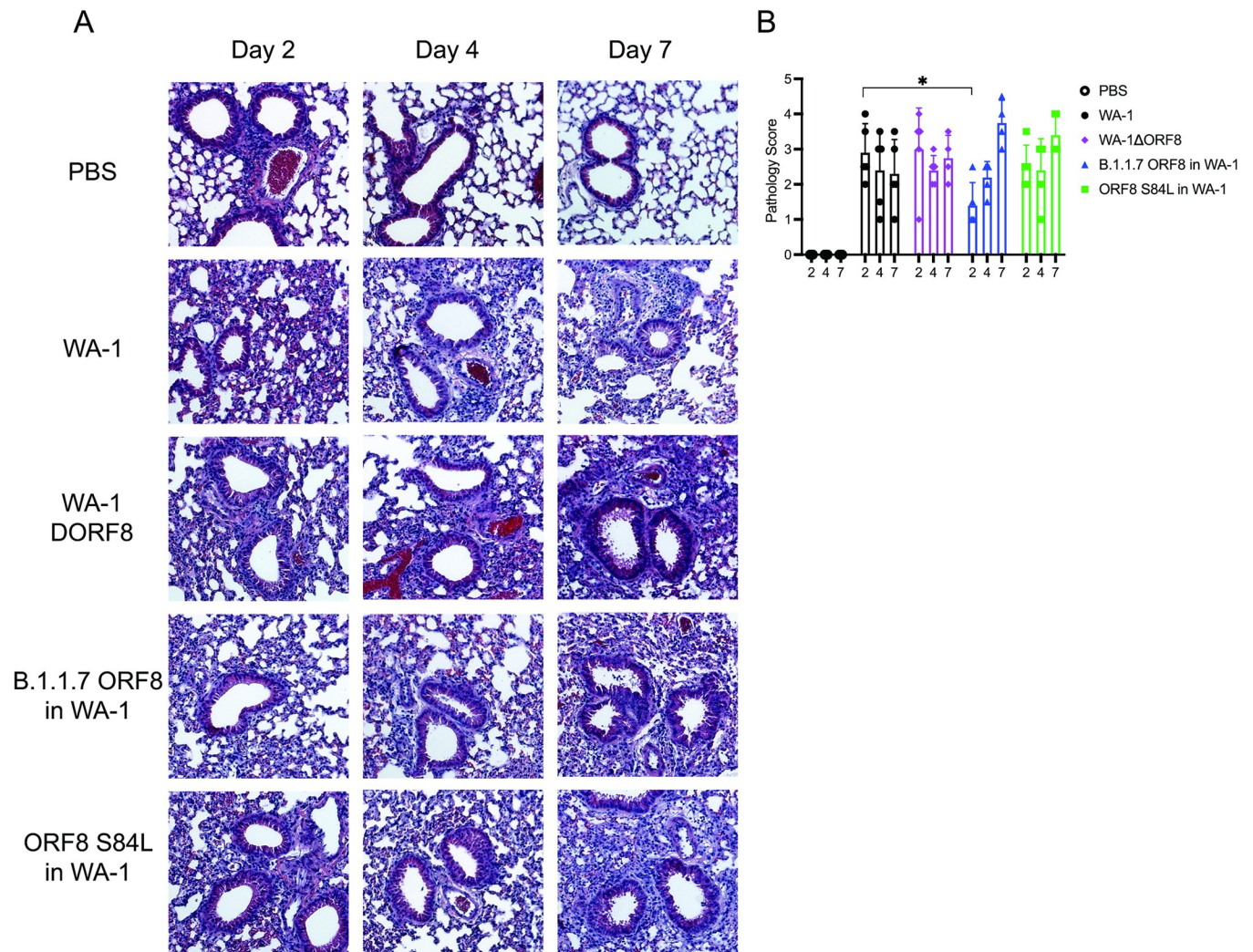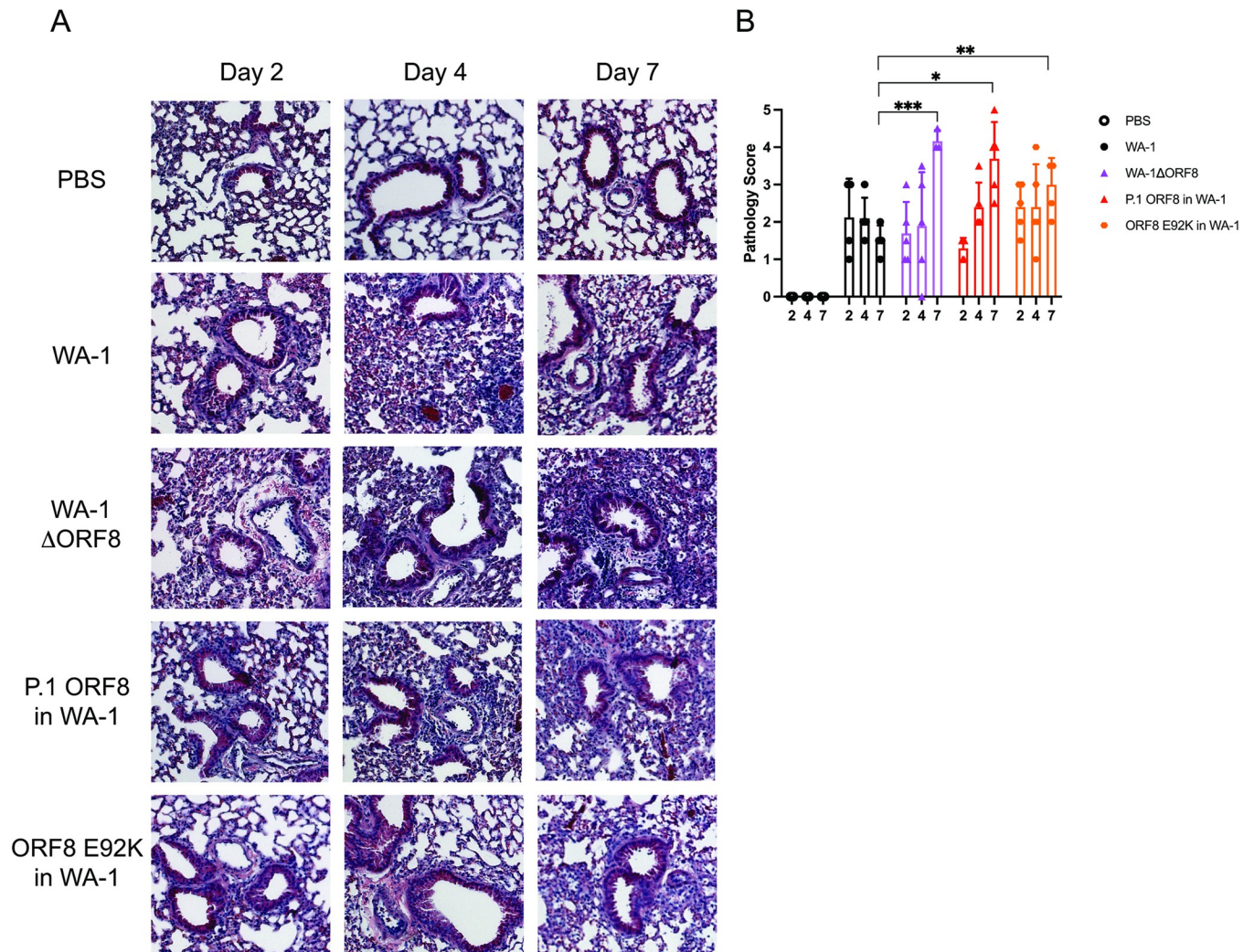
Fig 6. Lung histology and histological scores of mice infected with WA-1, WA-1ΔORF8, B. 1.1.7 ORF8 in WA-1, or ORF8 S84L in WA-1. Lungs from infected mice at day 2, 4 and 7 post infection were fixed and sectioned for staining with H&E. A. H&E staining of the lungs of mice infected with 10^3 PFU of WA-1, WA-1ΔORF8, B. 1.1.7 ORF8 in WA-1, or ORF8 S84L. Representative images shown of 5 mice per virus per timepoint. B. Histological scoring of the lungs of mice infected with either WA-1ΔORF8 or WA-1. Scoring described in methods section (n = 5 mice per timepoint). Sample comparisons with significant differences are shown. (*, p≤ 0.05; **, p≤0.005; ***, p≤0.0005).

https://doi.org/10.1371/journal.ppat.1011669.g006

exhibit increased thickening of the major airways and sloughing of the epithelial cells into the air space (**Fig 6A**). Lung inflammation was scored for each virus (**Fig 6B**). Intriguingly, the lungs of mice infected with the ORF8 S84L in WA-1 virus also resemble the lungs of mice infected with the deletion virus, with a skew towards more inflammation in the lungs (**Fig 6A**).

The lungs of the mice infected with the P.1 ORF8 containing virus and the ORF8 E92K containing virus scored consistently with the weight loss data seen in **Fig 7**. The lungs of the mice infected with the P.1 ORF8 virus exhibited an intermediate inflammatory phenotype compared to the mice infected with WA-1 and the mice infected with the WA-1ΔORF8 virus. We observe more inflammation in the alveolar space when compared to WA-1, but less thickening of the major airways compared to what is observed in the mice infected with the ORF8 deletion virus (**Fig 7A**). The lungs of the mice infected with the deletion virus were more inflamed than the lungs of mice infected with the wildtype virus, with a striking significantly higher

Fig 7. Lung histology and histological scores of mice infected with WA-1, WA-1ΔORF8, P.1 ORF8 in WA-1, or ORF8 E92K in WA-1. Lungs from infected mice at day 2, 4 and 7 post infection were fixed and sectioned for staining with H&E. A. H&E staining of the lungs of mice infected with 10^3 PFU of WA-1, WA-1ΔORF8, P.1 ORF8 in WA-1, or ORF8 E92K. Representative images shown of 5 mice per virus per timepoint. B. Histological scoring of the lungs of mice infected with WA-1, WA-1ΔORF8, P.1 ORF8 in WA-1, or ORF8 E92K. Scoring described in methods section (n = 5 mice per timepoint). Sample comparisons with significant differences are shown. (*, $p \leq 0.05$; **, $p \leq 0.005$; ***, $p \leq 0.0005$).

pathology score being seen at Day 7 (p = 0.00016; **Fig 7B**). The P.1 ORF8 virus infected mice also had significantly higher inflammation in the lungs at Day 7 (p = 0.0046) (**Fig 7B**). The lungs of the mice infected with the ORF8 E92K virus resembled the lungs of the mice infected with the WA-1 virus and did not achieve the levels of inflammation seen with the deletion virus and the P.1 ORF8 virus. However, at day 7, the lungs of these mice were more inflamed than the lungs of the mice infected with the wildtype virus (p = 0.0061; **Fig 7B**).

Discussion

Our work with both an ORF8 deletion virus and variant ORF8 viruses has revealed that this protein contributes to modulating the inflammation caused by SARS-CoV-2. Mice infected with the WA-1ΔORF8 virus showed significantly higher levels of inflammation in the lungs compared to mice infected with the wildtype virus. Our total RNA sequencing data from the

lungs of these mice revealed differential expression of genes involved in cytokine storm signaling pathways, macrophage activation pathways, and neutrophil signaling. In line with this RNA sequencing data, we saw a significant increase in the population of macrophages in the lungs of mice infected with the deletion virus compared to mice infected with the wildtype virus. We did not see a difference in the number of neutrophils in these lungs, suggesting that this is a cell-type specific phenomenon.

Previously published data suggests that the ORF8 of SARS-CoV-2 serves to downregulate MHCI, which presents antigen to CD8+ cytotoxic T cells.[9] Our cytokine array data did show an increase in the transcript for β2-microglobulin (β2m), which would corroborate this data. However, we did not see MHCI appear in our bulk RNA sequencing data. This could mean that the downregulation of MHCI is mostly at the protein level and not at the transcript level. We did see a significant upregulation in the amount of macrophages in the lungs of the deletion virus-infected mice compared to the wildtype-infected mice both by IHC and flow cytometric analysis. This may be due to signaling by the cytotoxic T cells, which secrete IFN-γ to activate macrophages.[19] Notably, both T cells and macrophages are known to play a significant role in the immune response of SARS-CoV-2.[20,21] In the mouse experiments, we see an interesting dose dependent effect where the higher dose of inoculum shows more significant differences in weight loss and lung pathology compared to the lower dose whereas the lower dose has greater differences in cytokine and chemokine changes by mRNA quantitation. We hypothesize this is due to the effect that ORF8 has on replication of SARS-CoV-2 in vivo and that the kinetics of replication and its interaction with the host response may be altering the mechanism of ORF8 and variant ORF8s in mice. To this point, we do see differences in interferon response genes in the transcriptome data suggesting that either ORF8 directly or the level of viral replication is differentially inducing a Type I IFN response. Further mechanistic studies are needed to determine the role of ORF8 in both replication and host immune response in the future.

Our work with the recombinant variant ORF8 viruses suggests that naturally occurring mutations in the SARS-CoV-2 ORF8 protein affect its function. As expected, the B.1.1.7 ORF8 in WA-1 mice exhibited increased weight loss and moderately increased inflammation in the lungs, which is unsurprising given that the ORF8 protein of the alpha lineage possesses a premature stop codon that truncates the protein 94 amino acids early. We have also shown that the mutation S84L, which is present in all of the variants, may serve to attenuate the function of ORF8, as mice infected with this virus and the P.1 ORF8 virus, which contains this mutation and an additional E92K mutation, appear to exhibit increased inflammation in the lungs compared to that caused by infection with the wildtype WA-1 virus. Current Omicron variants starting with the XBB lineage also have a mutated ORF8 with a stop codon at amino acid 8 (G8*) in the ORF[1]. This leads to a truncated protein, similar to the mutation seen in B.1.1.7 where ORF8 is truncated at amino acid 27. Based on our data, the truncation in all XBB lineages should also lead to increased inflammation, which can result in beneficial or detrimental phenotypes in humans depending on the other mutations in the genome. Understanding how the individual mutations function by themselves as well as when combined with other mutations in the SARS-CoV-2 genome can help to predict the pathogenesis of future variants.

The predominant ORF8 mutation S84L arose early in the virus' circulation. It is interesting to note that there were two predominant circulating strains of the original SARS-CoV-2 virus in Wuhan, China.[22,23] These two strains were known as the S strain and the L strain, which were named for the amino acid they coded in the ORF8 protein. Interestingly, the L strain was attributed to more disease severity, which is corroborated by our data here. Given that the S strain gave rise to the L strain and the L strain is associated with more severe disease, it appears that there is some selective pressure on this ORF8 mutation that led to loss of function. It

should be noted that the accessory protein ORF8 is the most highly divergent accessory ORF when compared to the ORF8 proteins of SARS-CoV. The SARS-CoV ORF8 possesses a 29-nucleotide deletion that functionally splits the ORF8 region into two smaller proteins, ORF8a and ORF8b.[24] Given our work and other published data, it appears that the loss of function of the ORF8 protein of SARS-CoV-2 has occurred independently throughout the evolution of the virus, suggesting that this loss of function is advantageous to the virus.[25–28] Further studies aim to directly compare the S and L strains of Wuhan-1, characterize the differences in inflammation seen with the variant ORF8 proteins, and further investigate naturally occurring truncations and deletions in ORF8 and their effects on viral pathogenesis.

Supporting information

S1 Fig. A gating diagram is shown for the flow cytometry results in Fig 4. All antibodies are identified in the methods section. The ezhic cell population shown in Fig 4 are macrophages, which for this gating strategy are CD45$^+$/Ly6G$^-$/CD11b$^+$/CD64$^+$. The labels on the axis are the antibodies used in that gating and the label at the top of each box is the population of cells gated from the previous box.
(TIF)

Acknowledgments

Author Contributions

Conceptualization: Marisa E. McGrath, Sanjay Vashee, Matthew B. Frieman.

Data curation: Marisa E. McGrath, Carly Dillen, Jeremy Ardanuy, Matthew B. Frieman.

Formal analysis: Marisa E. McGrath, Carly Dillen, Norberto Gonzalez-Juarbe, Matthew B. Frieman.

Funding acquisition: Sanjay Vashee, Matthew B. Frieman.

Investigation: Marisa E. McGrath, Louis Taylor, Carly Dillen, Jeremy Ardanuy, Norberto Gonzalez-Juarbe, Lauren Baracco, Raymond Kim, Rebecca Hart, Nacyra Assad-Garcia, Matthew B. Frieman.

Methodology: Marisa E. McGrath, Yong Xue, Louis Taylor, Jeremy Ardanuy, Norberto Gonzalez-Juarbe, Lauren Baracco, Raymond Kim, Rebecca Hart, Nacyra Assad-Garcia, Sanjay Vashee, Matthew B. Frieman.

Resources: Matthew B. Frieman.

Supervision: Matthew B. Frieman.

Validation: Matthew B. Frieman.

Writing – original draft: Marisa E. McGrath, Matthew B. Frieman.

Writing – review & editing: Marisa E. McGrath, Matthew B. Frieman.

References

1. CDC. CDC Museum COVID-19 Timeline. In: Centers for Disease Control and Prevention [Internet]. 16 Aug 2022 [cited 9 Jan 2023]. Available: https://www.cdc.gov/museum/timeline/covid19.html

2. COVID-19 Map. In: Johns Hopkins Coronavirus Resource Center [Internet]. [cited 9 Jan 2021]. Available: https://coronavirus.jhu.edu/map.html

3. A Novel Coronavirus from Patients with Pneumonia in China, 2019 | NEJM. [cited 23 Feb 2022]. Available: https://www.nejm.org/doi/full/10.1056/nejmoa2001017

4. Hu B, Guo H, Zhou P, Shi Z-L. Characteristics of SARS-CoV-2 and COVID-19. Nat Rev Microbiol. 2021; 19: 141–154. https://doi.org/10.1038/s41579-020-00459-7 PMID: 33024307

5. Mittal A, Manjunath K, Ranjan RK, Kaushik S, Kumar S, Verma V. COVID-19 pandemic: Insights into structure, function, and hACE2 receptor recognition by SARS-CoV-2. PLoS Pathog. 2020; 16: e1008762. https://doi.org/10.1371/journal.ppat.1008762 PMID: 32822426

6. Fang P, Fang L, Zhang H, Xia S, Xiao S. Functions of Coronavirus Accessory Proteins: Overview of the State of the Art. Viruses. 2021; 13: 1139. https://doi.org/10.3390/v13061139 PMID: 34199223

7. Redondo N, Zaldívar-López S, Garrido JJ, Montoya M. SARS-CoV-2 Accessory Proteins in Viral Pathogenesis: Knowns and Unknowns. Front Immunol. 2021; 12: 708264. https://doi.org/10.3389/fimmu.2021.708264 PMID: 34305949

8. Wong HH, Fung TS, Fang S, Huang M, Le MT, Liu DX. Accessory proteins 8b and 8ab of severe acute respiratory syndrome coronavirus suppress the interferon signaling pathway by mediating ubiquitin-dependent rapid degradation of interferon regulatory factor 3. Virology. 2018; 515: 165–175. https://doi.org/10.1016/j.virol.2017.12.028 PMID: 29294448

9. The ORF8 protein of SARS-CoV-2 mediates immune evasion through down-regulating MHC- | PNAS. [cited 9 Jan 2023]. Available: https://www.pnas.org/doi/10.1073/pnas.2024202118

10. Chou J-M, Tsai J-L, Hung J-N, Chen I-H, Chen S-T, Tsai M-H. The ORF8 Protein of SARS-CoV-2 Modulates the Spike Protein and Its Implications in Viral Transmission. Frontiers in Microbiology. 2022; 13. Available: https://www.frontiersin.org/articles/10.3389/fmicb.2022.883597 PMID: 35663899

11. Wu X, Xia T, Shin W-J, Yu K-M, Jung W, Herrmann A, et al. Viral Mimicry of Interleukin-17A by SARS-CoV-2 ORF8. mBio. 2022; e0040222. https://doi.org/10.1128/mbio.00402-22 PMID: 35343786

12. Su YCF, Anderson DE, Young BE, Linster M, Zhu F, Jayakumar J, et al. Discovery and Genomic Characterization of a 382-Nucleotide Deletion in ORF7b and ORF8 during the Early Evolution of SARS-CoV-2. mBio. 2020; 11: 10.1128/mbio.01610-20. https://doi.org/10.1128/mBio.01610-20 PMID: 32694143

13. McGrath ME, Xue Y, Dillen C, Oldfield L, Assad-Garcia N, Zaveri J, et al. SARS-CoV-2 Variant Spike and accessory gene mutations alter pathogenesis. 2022. https://doi.org/10.1101/2022.05.31.494211 PMID: 35677080

14. Gibson DG, Glass JI, Lartigue C, Noskov VN, Chuang R-Y, Algire MA, et al. Creation of a bacterial cell controlled by a chemically synthesized genome. Science. 2010; 329: 52–56. https://doi.org/10.1126/science.1190719 PMID: 20488990

15. Martin M. Cutadapt removes adapter sequences from high-throughput sequencing reads. EMBnet.journal. 2011; 17: 10–12. https://doi.org/10.14806/ej.17.1.200

16. Dobin A, Davis CA, Schlesinger F, Drenkow J, Zaleski C, Jha S, et al. STAR: ultrafast universal RNA-seq aligner. Bioinformatics. 2013; 29: 15–21. https://doi.org/10.1093/bioinformatics/bts635 PMID: 23104886

17. Love MI, Huber W, Anders S. Moderated estimation of fold change and dispersion for RNA-seq data with DESeq2. Genome Biol. 2014; 15: 550. https://doi.org/10.1186/s13059-014-0550-8 PMID: 25516281

18. RStudio | Open source & professional software for data science teams. [cited 8 Jul 2022]. Available: https://www.rstudio.com/

19. Charles A Janeway J, Travers P, Walport M, Shlomchik MJ. T cell-mediated cytotoxicity. Immunobiology: The Immune System in Health and Disease 5th edition. 2001 [cited 12 Mar 2023]. Available: https://www.ncbi.nlm.nih.gov/books/NBK27101/

20. Merad M, Martin JC. Pathological inflammation in patients with COVID-19: a key role for monocytes and macrophages. Nat Rev Immunol. 2020; 20: 355–362. https://doi.org/10.1038/s41577-020-0331-4 PMID: 32376901

21. de Candia P, Prattichizzo F, Garavelli S, Matarese G. T Cells: Warriors of SARS-CoV-2 Infection. Trends Immunol. 2021; 42: 18–30. https://doi.org/10.1016/j.it.2020.11.002 PMID: 33277181

22. Cheng X, Li J, Zhang L, Hu W, Zong L, Xu X, et al. Identification of SARS-CoV-2 Variants and Their Clinical Significance in Hefei, China. Frontiers in Medicine. 2022; 8. Available: https://www.frontiersin.org/articles/10.3389/fmed.2021.784632 PMID: 35083244

23. Tang X, Wu C, Li X, Song Y, Yao X, Wu X, et al. On the origin and continuing evolution of SARS-CoV-2. National Science Review. 2020; 7: 1012–1023. https://doi.org/10.1093/nsr/nwaa036 PMID: 34676127

24. Muth D, Corman VM, Roth H, Binger T, Dijkman R, Gottula LT, et al. Attenuation of replication by a 29 nucleotide deletion in SARS-coronavirus acquired during the early stages of human-to-human transmission. Sci Rep. 2018; 8: 15177. https://doi.org/10.1038/s41598-018-33487-8 PMID: 30310104

25. Young BE, Fong S-W, Chan Y-H, Mak T-M, Ang LW, Anderson DE, et al. Effects of a major deletion in the SARS-CoV-2 genome on the severity of infection and the inflammatory response: an observational cohort study. The Lancet. 2020; 396: 603–611. https://doi.org/10.1016/S0140-6736(20)31757-8 PMID: 32822564

26. Brandt D, Simunovic M, Busche T, Haak M, Belmann P, Jünemann S, et al. Multiple Occurrences of a 168-Nucleotide Deletion in SARS-CoV-2 ORF8, Unnoticed by Standard Amplicon Sequencing and Variant Calling Pipelines. Viruses. 2021; 13: 1870. https://doi.org/10.3390/v13091870 PMID: 34578452

27. Akaishi T, Fujiwara K, Ishii T. Insertion/deletion hotspots in the Nsp2, Nsp3, S1, and ORF8 genes of SARS-related coronaviruses. BMC Ecology and Evolution. 2022; 22: 123. https://doi.org/10.1186/s12862-022-02078-7 PMID: 36307763

28. Mazur-Panasiuk N, Rabalski L, Gromowski T, Nowicki G, Kowalski M, Wydmanski W, et al. Expansion of a SARS-CoV-2 Delta variant with an 872 nt deletion encompassing ORF7a, ORF7b and ORF8, Poland, July to August 2021. Euro Surveill. 2021; 26: 2100902. https://doi.org/10.2807/1560-7917.ES.2021.26.39.2100902 PMID: 34596017